Desalination and Water Treatment
www.deswater.com
doi: 10.5004/dwt.2021.26931

218 (2021) 135–145
April

Modeling and investigation of operating parameters on thermal performance of a hollow fiber membrane in DCMD

Sepehr Nikkho[a], Jafar Zahirifar[a], Javad Karimi-Sabet[b,*], Abolfazl Dastbaz[a], Alireza Hadi[a]

[a]*Department of Chemical Engineering, Faculty of Engineering, University of Tehran, P.O. Box: 14395-983, Tehran, Iran, emails: nikkho.sepehr@ut.ac.ir (S. Nikkho), jafar.zahiri@ut.ac.ir (J. Zahirifar), a.dastbaz@ut.ac.ir (A. Dastbaz), alireza68hadi@gmail.com (A. Hadi)*
[b]*Material and Nuclear Fuel Research School (MNFRS), Nuclear Science and Technology Research Institute, Tehran, Iran, Tel. +98 (21) 88221117; email: j_karimi@alum.sharif.edu*

Received 29 June 2020; Accepted 14 December 2020

ABSTRACT

In this study, numerical models are introduced for measuring and estimating water flux in direct contact membrane distillation through hollow fiber module. The experimental data (from the commercial polypropylene hollow fiber membrane) are used to measure the mass transfer coefficients of the membrane. Then, Knudsen diffusion-molecular diffusion-Poiseuille flow transition parameters are estimated by implementing the non-linear regression analysis via MATLAB software. Afterward, the validation of models is acquired via comparison with the experimental data. Finally, the influence of the operating parameters (temperature and velocity) on water flux, heat convection coefficient, temperature polarization coefficient, thermal efficiency, and specific energy consumption is investigated.

Keywords: Direct contact membrane distillation; Hollow fiber membrane; Heat/mass transfer mechanism; Temperature polarization coefficient; Thermal efficiency; Specific energy consumption

1. Introduction

The growing scarcity of drinking water is becoming a serious menace for the human being in the present era. On the other hand, the increasing necessity for freshwater owing to population explosion, industrial and agricultural activities, and economic growth has deteriorated the crisis of water shortage [1,2]. Approximately 98% of the water on the earth is brackish water; thereby desalination of saline water through desalination techniques plays a crucial role in tackling the problem of water scarcity [3]. Among various desalination approaches, membrane distillation (MD) is regarded as a viable alternative for producing freshwater due to its superior characteristics [4].

MD process is a combination of thermal distillation and membrane operation whereby heat and mass transfer phenomena happen simultaneously within the membrane. This process consists of three stages: (1) partial evaporation of hot saline solution at the interface between feed and membrane in feed side; (2) diffusion of vapor in the porous hydrophobic membrane; (3) condensation and collection of vapor in permeate side [5]. The partial vapor pressure gradient is the driving force in MD which is triggered by temperature gradient across the membrane. The principal merits of MD compared to other conventional desalination processes like reverse osmosis (RO) include (1) lower operating temperature and pressure; (2) less prone to fouling; (3) approximately 100% removal of non-volatile constituents; (4) less sensitive to feed variations such as pH and concentration; and (5) lower energy consumption [6,7].

With respect to how transferred vapors are gathered, MD can be categorized into four various configurations

* Corresponding author.

including direct contact membrane distillation (DCMD), air gap membrane distillation (AGMD), vacuum membrane distillation (VMD), and sweeping gas membrane distillation (SGMD). DCMD is the simplest, easiest, most used, and the best configuration for the removal of volatile constituents in MD projects, however, it has the highest heat loss and temperature polarization among different MD modes. In AGMD, heat loss and membrane fouling are remarkably low, however, due to the existence of stagnant air which causes supplementary mass transfer resistance, mass flux is low. Due to the application of condenser and vacuum pump, VMD is considered as a high-cost mode. But in this configuration, temperature polarization is very low, and mass flux is high. SGMD has the lowest temperature polarization, however, mass flux is low, pretreatment of sweeping gas is essential, and like VMD mode owing to the application of equipment such as blower and condenser, the overall cost is high [8,9].

In MD process, three various membrane modules are offered: (1) flat sheet; (2) spiral; and (3) hollow fiber. Among diverse types of membrane modules, hollow fiber membrane (HFM) modules have obtained noticeable attention due to their unique characteristics such as high packing density, low-temperature polarization, high mass and heat transfer, feasible scale-up, no necessity for supplementary structure, and its potential for industrial usage. Despite substantial experimental researches conducted on HFM, only few projects concerning the modeling of HFM processes have been conducted which can be due to the complicated conditions in MD technology [4,10,11]. Yazgan-Birgi et al. [12] offered three-dimensional (3D) CFD models for flat-sheet and HF membranes with application to the DCMD process. Then, the models were validated through the experimental results, and finally, the effects of various operating parameters on flux and temperature polarization coefficient (TPC) were investigated. In their results, HFM process indicated lower flux compared to flat sheet membranes, and they concluded that operating parameters have significant effects on flux and TPC [12]. Yu et al. [13] proposed a two-dimensional (2D) computational fluid dynamics (CFD) heat transfer model for DCMD under laminar conditions and counter-current flow. They evaluated the mass and heat transfer phenomena via proposed model and studied the hydrodynamic conditions in a single HF module. Yu et al. [14] used the same model to evaluate the performance of HFM process with different mass flux coefficients through HF modules with and without baffles. They investigated the influence of operating parameters on heat and mass transfer for DCMD and concluded that at higher temperatures, a baffled module showed a better performance in comparison to a non-baffled module. Cheng et al. [15] used mass, energy, and momentum balances on the feed and permeate sides to evaluate the variations of operating parameters, flux, TPC, etc., along the fiber length in the hollow fiber module for DCMD [15]. However, up to present, modeling of HFM in DCMD process through Knudsen diffusion-molecular diffusion-Poiseuille flow transition (KMPT) parameters has not been reported yet.

Therefore, in this research, experimental results were applied to develop a predictive model for DCMD process. After developing the theoretical heat and mass balance, the mass transfer coefficients (MTC) of the membrane at various temperatures and velocities were determined. Then, KMPT parameters (C_K, C_M, and C_P) were measured via non-linear regression approach using MATLAB software. Afterward, the experimental data at various temperatures and velocities were compared with the results obtained from the introduced models. Finally, using the validated models, the impact of the operating parameters including feed temperature and velocity were investigated. The results indicated that operating parameters had a significant influence on water flux, heat convection coefficient, TPC, TE, and SEC.

2. Theory

MD process is a complex separation technology in which mass and heat transfer happen simultaneously. In Fig. 1, an outline of the DCMD set-up used in this study is depicted. In the HF module, a number of the membrane fibers are attached to the membrane shell. A scheme of the HF module is shown in Fig. 2a. In the HF module, the feed and permeate flows were under counter-current flow in lumen and shell sides, respectively. Figs. 2b and c illustrate the heat and mass transfer model applied for the distillation operation, respectively. The operating conditions for DCMD experiments are reported in Table 1. As listed in Table 2, the properties of the membrane applied in the DCMD process are presented and the principal assumptions applied in this work are as follows:

- Steady-state condition
- No chemical reaction takes place
- The membrane properties are constant
- No heat loss to the environment

2.1. Heat and mass transfer in HFM for DCMD

2.1.1. Heat transfer

- Heat transfer through the feed flow on the lumen side

$$Q^F = h^F\left(\pi N d_i\right)\left(T^F - T_m^F\right) \tag{1}$$

In Eq. (1), N is the number of fibers, d_i is the internal diameter of the fiber, T^F is the bulk temperature of the feed flow, T_m^F is the temperature of the membrane surface on the feed side, and h^F is the convective heat transfer coefficient on the feed side that can be measured through the Nusselt number (Nu) as presented by the following equations:

$$\mathrm{Nu}^F = \frac{h^F d_i}{k^F} = 1.62\left(\mathrm{Re}^F\,\mathrm{Pr}^F\,\frac{d_i}{L}\right)^{0.33} \qquad \mathrm{Re}^F < 2{,}100 \tag{2}$$

$$\mathrm{Nu}^F = \frac{h^F d_i}{k^F} = 0.023\left(\mathrm{Re}^F\right)^{0.8}\left(\mathrm{Pr}^F\right)^{0.33} \qquad \mathrm{Re}^F > 2{,}100 \tag{3}$$

where k^F is the feed thermal conductivity, L is the length of the fiber, Re^F is the Reynolds number associated with the feed side, and Pr^F is the Prandtl number on the feed side. Prandtl and Reynolds numbers are defined based on the following equations:

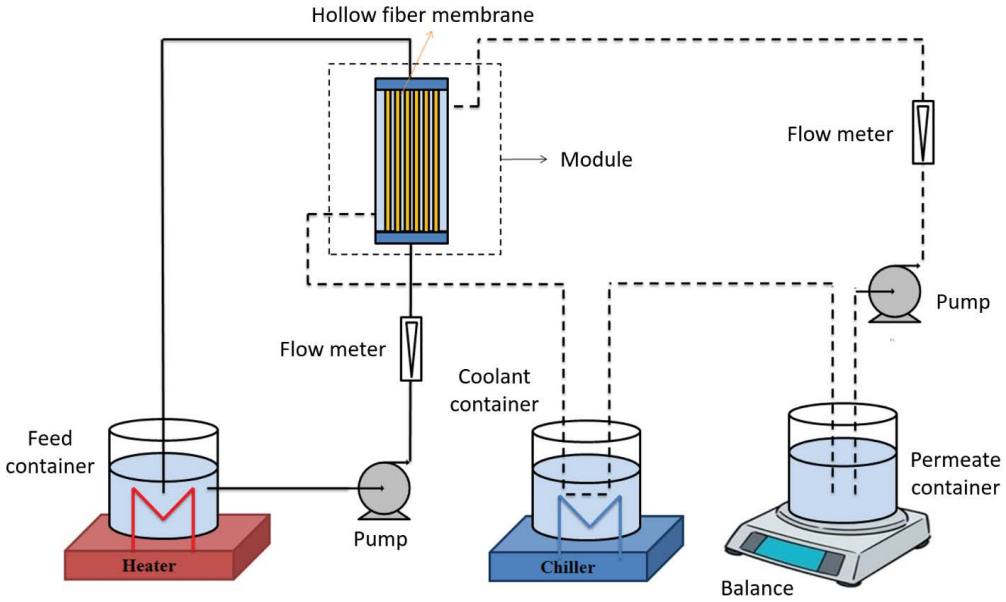

Fig. 1. Schematic diagram of the DCMD set-up.

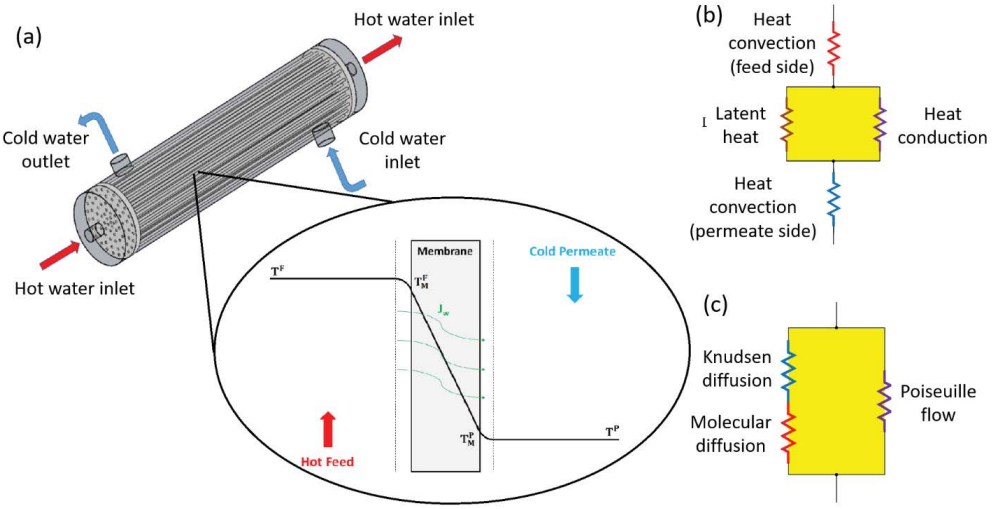

Fig. 2. (a) Schematic diagram of the counter-current HF module, (b) heat transfer resistances for the energy transfer in DCMD process, and (c) mass transfer model in DCMD process for gas transfer through the HF membrane (yellow color).

$$\mathrm{Re}^F = \frac{\rho^F u^F d_i}{\mu^F} \tag{4}$$

$$\mathrm{Pr}^F = \frac{C_p^F \mu^F}{k^F} \tag{5}$$

where ρ^F, u^F, C_p^F, and μ^F are density, velocity, specific heat capacity, and viscosity of the feed flow, respectively.

- Heat transfer for permeate flow on the shell side

$$Q^P = h^P \left(\pi N d_o\right)\left(T_m^P - T^P\right) \tag{6}$$

Table 1
Operating conditions used in DCMD process

Parameter	Value
Inlet feed temperature (°C)	35–55
Inlet permeate temperature (°C)	29
Inlet feed flow rate (L/h)	50–150
Inlet carrier flow rate (L/h)	50

In Eq. (6), d_o is the external diameter of the fiber, T_m^P is the temperature of the membrane surface on the permeate side, T^P is the bulk temperature on the permeate side, and h^P is the convective heat transfer coefficient on the

Table 2
Properties of membrane applied for the DCMD process

Parameter	Value
d_i (mm)	1.8
d_0 (mm)	2.7
Fiber length (m)	0.45
Shell diameter (m)	0.021
Membrane porosity	0.73
Thickness (mm)	0.45
Pore radius (μm)	0.1
Number of fibers	40
Membrane thermal conductivity (W/m K)	0.17

permeate side which can be determined through the Nusselt number as:

$$\mathrm{Nu}^P = \frac{h^P d_h}{k^P} = 0.023\left(\mathrm{Re}^P \cos\theta\right)^{0.8}\left(\mathrm{Pr}^P\right)^{0.33} \tag{7}$$

where k^P is the permeate thermal conductivity, θ is the yaw angle which for the cross-flow is 0° and for the parallel flow is 90°, d_h is the hydraulic diameter of the shell, Re^P and Pr^P are the Reynolds and Prandtl numbers on the permeate side. Reynolds and Prandtl numbers on the shell side are defined according to the following equations:

$$\mathrm{Re}^P = \frac{\rho^P u^P d_h}{\mu^P} \tag{8}$$

$$\mathrm{Pr}^P = \frac{C_p^P \mu^P}{k^P} \tag{9}$$

Where ρ^P, u^P, C_p^P, and μ^P are density, velocity, specific heat capacity, and viscosity of the permeate flow, respectively. The following equations are proposed to calculate the water flow properties, including density (ρ_w), thermal conductivity (k_w), viscosity (μ_w), and specific heat capacity ($C_{p,w}$).

$$\rho_w = 999.8425 + 6.7939\times10^{-2}T - 9.0953\times10^{-3}T^2 + 1.0017 \times10^{-4}T^3 - 1.1201\times10^{-6}T^4 + 6.5363\times10^{-9}T^5$$
T in °C (10)

$$k_w = -0.9225 + 2.8395\left(\frac{T}{273.15}\right) - 1.8007\left(\frac{T}{273.15}\right)^2 + 0.5258\left(\frac{T}{273.15}\right)^3 - 0.0734\left(\frac{T}{273.15}\right)^4$$
T in K (11)

$$C_{p,w} = 4,217.4 - 3.72T + 0.141T^2 - 2.654\times10^{-3}T^3 + 2.093\times10^{-5}T^4$$
T in °C (12)

$$\mu_w = 2.414\times10^{-5}\times10^{\left(\frac{247.8}{T-140}\right)}$$
T in K (13)

Moreover, the hydraulic diameter of the shell which depends on the module packing density, is expressed according to the following equation:

$$d_h = \left(\frac{1-\Phi}{\Phi}\right)d_o \tag{14}$$

$$\Phi = N\left(\frac{d_o}{d_s}\right)^2 \tag{15}$$

In Eq. (14), Φ is defined as the packing density and d_s, in Eq. (15) is the internal diameter of the shell.

- Heat transfer across the membrane

As represented in Fig. 2b, the heat transfer across the membrane occurs via two various mechanisms including latent heat of water evaporation and thermal conduction. As these two mechanisms are in parallel, the equation describing the heat transfer across the membrane can be expressed according to the following equation:

$$Q^m = \left(\pi N d_{\mathrm{lm}}\right)\left[J\Delta H + \frac{k_m}{\delta_m}\left(T_m^F - T_m^P\right)\right] \tag{16}$$

$$d_{\mathrm{lm}} = \frac{d_o - d_i}{\ln\left(\frac{d_o}{d_i}\right)} \tag{17}$$

where J is permeate mass flux, ΔH is the latent heat of water evaporation, k_m is the membrane thermal conductivity, and δ_m is the membrane thickness. The membrane thickness (δ_m), membrane thermal conductivity (k_m), and latent heat of water evaporation (ΔH) are defined according to the following equations:

$$\delta_m = \frac{d_o - d_i}{2} \tag{18}$$

$$k_m = k_g\varepsilon + k_p\left(1-\varepsilon\right) \tag{19}$$

$$k_g = 0.0272 + 5.71\times10^{-6}\times T_m \tag{20}$$

$$\Delta H = 2,502.9 - 2.4292\left(T_m - 273.15\right) \tag{21}$$

In Eq. (19), ε is the membrane porosity, k_p is the thermal conductivity of the membrane material, and k_g is the thermal conductivity of the trapped air across the membrane

pores which are calculated at T_m. In Eqs. (20) and (21), T_m is expressed in Kelvin unit and is the arithmetic mean of T_m^F and T_m^P. According to the assumption of the steady-state condition:

$$Q^F = Q^P = Q^m$$

Thus, the membrane temperatures at the feed and permeate sides are obtained through the combination of Eqs. (1), (6), and (16) which can be expressed based on the following equations:

$$T_m^F = \frac{\left(1+\frac{h_P d_o \delta_m}{d_{\mathrm{lm}} k_m}\right)\left(\frac{h_F d_i \delta_m}{d_{\mathrm{lm}} k_m}\right) T_f - \left(1+\frac{h_P d_o \delta_m}{d_{\mathrm{lm}} k_m}\right)\left(\frac{J\Delta H \delta_m}{k_m}\right) + \left(\frac{h_P d_o \delta_m}{d_{\mathrm{lm}} k_m}\right) T_p + \left(\frac{J\Delta H \delta_m}{k_m}\right)}{\left(1+\frac{h_P d_o \delta_m}{d_{\mathrm{lm}} k_m}\right)\left(1+\frac{h_F d_i \delta_m}{d_{\mathrm{lm}} k_m}\right) - 1} \tag{22}$$

$$T_m^p = \frac{\left(1+\frac{h_F d_i \delta_m}{d_{\mathrm{lm}} k_m}\right)\left(\frac{h_P d_o \delta_m}{d_{\mathrm{lm}} k_m}\right) T_p + \left(1+\frac{h_F d_i \delta_m}{d_{\mathrm{lm}} k_m}\right)\left(\frac{J\Delta H \delta_m}{k_m}\right) + \left(\frac{h_F d_i \delta_m}{d_{\mathrm{lm}} k_m}\right) T_f - \left(\frac{J\Delta H \delta_m}{k_m}\right)}{\left(1+\frac{h_P d_o \delta_m}{d_{\mathrm{lm}} k_m}\right)\left(1+\frac{h_F d_i \delta_m}{d_{\mathrm{lm}} k_m}\right) - 1} \tag{23}$$

2.1.2. Mass transfer

Mass flux (J) acquired through the MD membrane is proportional to the vapor pressure gradient within the membrane, and consequently, the following correlation can be used to describe this dependency:

$$J = \Delta P_m = C\left(P_m^F - P_m^P\right) \tag{24}$$

In this Eq. (24), C is the mass transfer coefficient (MTC), and P_m^F and P_m^P are water vapor pressures on the membrane-feed and membrane-permeate interfaces which are dependent on T_m^F and T_m^P, respectively. The water vapor pressures at the membrane surface can be determined through Antoine equation as follows:

$$P_m = \exp\left[23.328 - \frac{3{,}816.44}{T_m - 45.24}\right] \tag{25}$$

The MTC can be measured through the KMPT model. In this model, the Knudsen diffusion accounts for the condition when the gas density is considerably low or the pore size is considerably small, and accordingly, the collision between gas molecules can be ignored. Additionally, the molecular diffusion explains the mass transfer when the molecule–molecule collisions are dominant compared to the molecule–wall collisions and also when various molecules diffuse towards lower concentrations. Furthermore, the gas flow as a continuous fluid driven by a pressure difference is attributed to the Poiseuille flow. As a result, the KMPT model is composed of Knudsen diffusion, molecular diffusion, and Poiseuille flow transition mechanisms [16,17]. There can be several configurations to arrange the three mechanisms. In the present model, as illustrated in Fig. 2c, the Knudsen gas resistance R_K and the molecular gas resistance R_M are in series and Poiseuille flow resistance R_P is in parallel with the other two resistances. Thus, the KMPT model is described as follows:

$$C = \left(R_k + R_M\right)^{-1} + R_P^{-1} \tag{26}$$

$$R_K^{-1} = \frac{r\varepsilon}{\tau\delta}\left(\frac{M_w}{RT_m}\right)^{0.5} = C_K\left(\frac{M_w}{RT_m}\right)^{0.5} \tag{27}$$

$$R_M^{-1} = \frac{\varepsilon}{\tau\delta}\left(\frac{DM_w}{Y_{\mathrm{lm}} RT_m}\right) = C_M\left(\frac{DM_w}{Y_{\mathrm{lm}} RT_m}\right) \tag{28}$$

$$R_M^{-1} = \frac{r^2\varepsilon}{\tau\delta}\left(\frac{P_m M_w}{\mu RT_m}\right) = C_P\left(\frac{P_m M_w}{\mu RT_m}\right) \tag{29}$$

$$J = \left[\frac{1}{\frac{1}{C_K\left(\frac{M_w}{RT_m}\right)^{0.5}} + \frac{1}{C_M\left(\frac{DM_w}{Y_{\mathrm{lm}} RT_m}\right)}} + C_P\left(\frac{P_w M_w}{\mu RT_m}\right)\right]\left(P_m^F - P_m^P\right) \tag{30}$$

$$C = \left[\frac{1}{\frac{1}{C_K\left(\frac{M_w}{RT_m}\right)^{0.5}} + \frac{1}{C_M\left(\frac{DM_w}{Y_{\mathrm{lm}} RT_m}\right)}} + C_P\left(\frac{P_w M_w}{\mu RT_m}\right)\right] \tag{31}$$

In the Eqs. (26)–(31), C_K, C_M, and C_P are the parameters of KMPT model, M_w, is molecular weight of water, R is ideal gas constant, ε is the membrane porosity, δ is the membrane thickness, r is the radius of the membrane pore, and τ is the membrane tortuosity. The pore radius of the membrane was calculated through bubble point method. Moreover, the membrane tortuosity (τ), and membrane porosity (ε), can be obtained according to the following equations:

$$\tau = \frac{\left(2-\varepsilon\right)^2}{\varepsilon} \tag{32}$$

$$\varepsilon = \frac{\text{wet membrane} - \text{dry membrane}}{\rho \mathrm{Al}} \tag{33}$$

$$A = \frac{\pi\left(d_o^2 - d_i^2\right)}{4} \tag{34}$$

where wet membrane is the weight of wet membrane, dry membrane is the weight of dry membrane, ρ is the liquid density, A is the membrane surface area, l is the length of membrane, and isopropyl alcohol was chosen as the wetting liquid. In Eq. (28), D is the water vapor diffusion coefficient and Y_{lm} is the log-mean mole fraction of the trapped air in the membrane pores. In Eq. (29), P_m is the mean value of P_m^F and P_m^P, and μ is the viscosity of water calculated under the membrane temperature T_m. This parameter can be calculated using water vapor pressures at the membrane-feed and membrane-permeate interfaces (P_m^F and P_m^P):

$$D = 1.19 \times 10^{-4} \left(\frac{T_m^{1.75}}{P_m} \right) \tag{35}$$

$$Y_{lm} = \left(\frac{\left(1 - \frac{P_m^F}{P_t}\right) - \left(1 - \frac{P_m^P}{P_t}\right)}{\ln\left(1 - \frac{P_m^F}{P_t}\right) - \ln\left(1 - \frac{P_m^P}{P_t}\right)} \right) \tag{36}$$

In Eq. (36), P_t represents the total pressure within the membrane pores.

3. Results and discussion

3.1. Influence of the operating parameters and model validation

With the aid of the experimental results obtained from the work of Perfilov et al. [18] for water flux at various feed temperatures and velocities, the MTC values for PP membrane under different temperatures and velocities were determined as follows:

- Calculating the heat transfer coefficients of the film on the feed and permeate side, h_F and h_P, respectively
- Calculating the temperatures in the layers adjacent to the membrane surface T_m^F and T_m^P
- Calculating the pressures in the layers adjacent to the membrane surface P_m^F and P_m^P
- Obtaining the model prediction of MTC values under various feed temperatures and velocities

Then, the C_K, C_M, and C_P values at various temperatures and velocities were obtained by non-linear regression analysis via MATLAB software. The values of experimental and calculated water flux, MTC, and KMPT parameters (C_K, C_M, and C_P) at different temperatures and velocities are shown in Tables 3 and 4. Moreover, the values of experimental and calculated water flux at various feed temperatures and velocities are shown in Figs. 3a and b. The comparison between experimental and calculated results for PP HFM indicates a fitting agreement between the model and experimental results which confirms the validation of the KMPT model.

Following the validation of the KMPT model, the influence of feed temperature and velocity variations on water flux was investigated. Based on Fig. 3a, the water flux indicates an increasing trend vs. temperature increase. This trend is owing to the influence of temperature on the partial vapor pressure. According to Eq. (24), water flux (J) is proportional to the MTC parameter, P_m^F and P_m^P (water vapor pressure on the membrane-feed and membrane-permeate interfaces). As listed in Table 3, increasing the temperature results in a rise in the MTC parameter. On the other hand, P_m^F and P_m^P are dependent on the temperature through Antoine Eq. (25). Thus, water flux rises exponentially with increasing the temperature [19].

Based on Fig. 3b, the water flux rises with increment in feed flow rate. This behavior is attributed to the increased turbulency generated as a result of increased velocity. The turbulent flow increases the mixing phenomenon through the feed flow, and consequently, reduces the thickness of the thermal boundary layer and increases the temperature on the feed side of the membrane. Thus, the increase in vapor pressure occurs and the water mass flux rises and the overall outcome of these effects is an

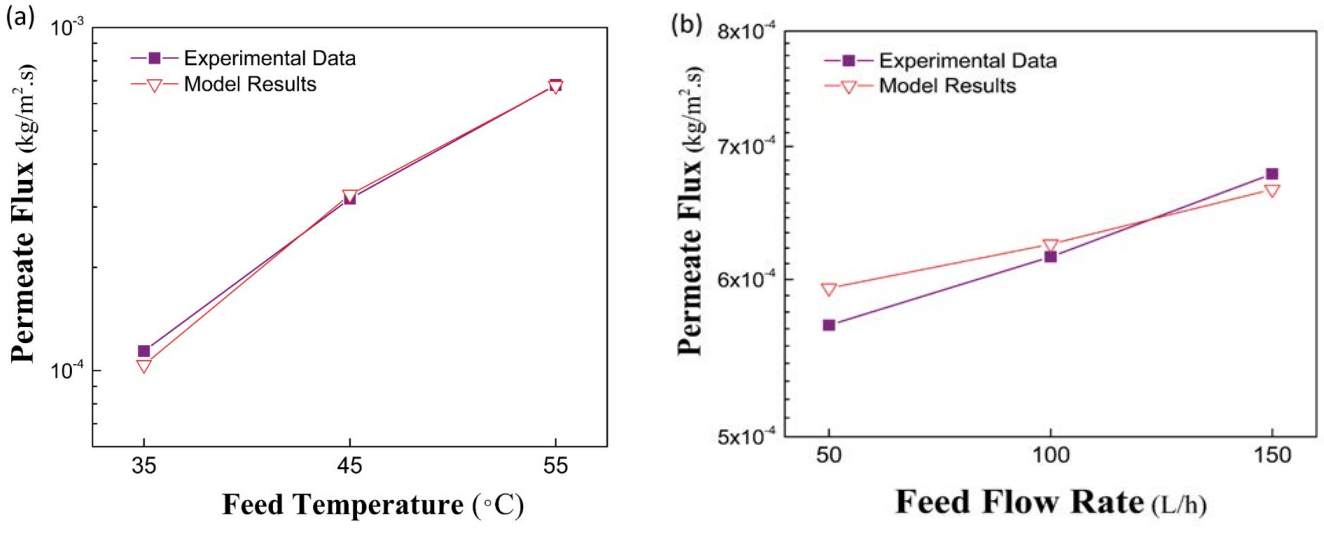

Fig. 3. Comparison between experimental and calculated water flux at various: (a) feed temperatures and (b) velocities.

Table 3
KMPT parameters and the comparison between experimental and model results for PP membrane

Temperature (°C)	MTC (10^{-7} kg/m^2 s pa)		Water flux (10^{-4} kg/m^2 s)	
	Measured	Calculated	Measured	Calculated
35	0.89	0.92	1.14	1.04
45	0.93	0.97	3.17	3.26
55	1.10	1.08	6.80	6.77

Values of the KMPT parameters: $C_K = 0.09$, $C_M = 18.16$, and $C_P = 8.55 \times 10^{-12}$.

increment in water mass flux and decrement in temperature polarization [20].

3.2. Heat convection coefficient

In this section, the effect of feed temperature and flow rate on the heat convection coefficient is studied. On the shell side, the carrier flow rate (50 L/h) is remarkably higher than the permeate flow rate and even though changing the feed flow parameters leads to a different permeate flow rate, the difference would be negligible compared with the carrier flow rate. Since the Re^P number depends on the flow velocity, it would remain approximately constant with increasing the feed flow rate, and as a result, the Nu^P number and h^P remain constant. On the other side of the membrane, as depicted in Fig. 4a, the heat convection coefficient (h^F) increases 2.2% with the increment of the feed temperature from 35°C to 55°C. This behavior can be attributed to the decreased viscosity of the feed flow as a result of a increase in the temperature. As the temperature rises, the liquid viscosity would decrease and as described in Eq. (4), this would lead to increased Re number which based on Eqs. (2) and (3), contributes to an increase in the Nu number and consequently, heat convection coefficient. Additionally, as shown in Fig. 4b, increasing the feed flow rate from 50 to 150 L/h leads to a 43.7% increase in the heat convection coefficient. Increasing the feed flow rate contributes to the velocity increment, and as result, the Re, Nu, and consequently, the heat convection coefficient would increase. Comparison of the results (Figs. 4a and b), highlights the superior effect of the feed flow rate compared with the feed temperature on the heat convection coefficient.

3.3. Temperature polarization coefficient

The temperature gradient between the surface temperature of the membrane and bulk temperature of feed and permeates flows is a result of the temperature polarization effect. As heat is transferred from the bulk feed through the boundary layer to the membrane surface on the feed side, the temperature polarization leads to the temperature on the surface of the membrane to be different from the temperature of the bulk flow. The same phenomenon is responsible for the temperature gradient on the permeate side of the membrane. The temperature polarization phenomenon is identified as one of the challenges accountable for limiting DCMD mass flux decay. The temperature polarization leads to the temperature gradient between (T^F and T_m^F) and (T^P and T_m^P). The value of the TPC is measured through the following equation:

$$\mathrm{TPC} = \frac{T_m^F - T_m^P}{T^F - T^P} \tag{37}$$

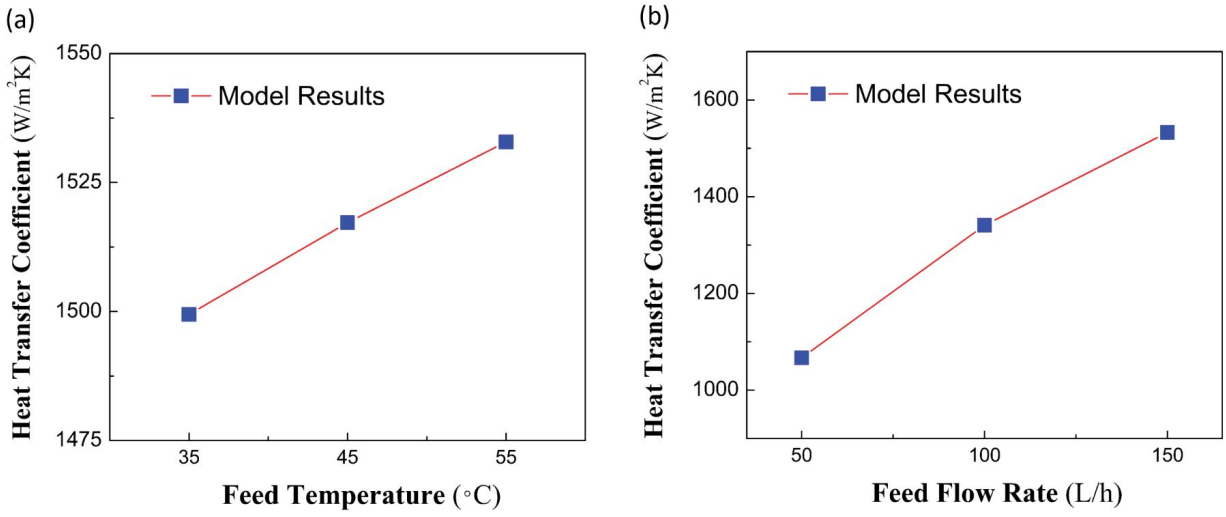

Fig. 4. Effect of (a) feed temperature and (b) velocity on the heat transfer coefficient.

Table 4
KMPT parameters and the comparison between experimental and model results for PP membrane

Feed flow rate (L/h)	MTC (10^{-7} kg/m^2 s pa)		Water flux (10^{-4} kg/m^2 s)	
	Measured	Calculated	Measured	Calculated
50	0.83	0.86	5.69	5.94
100	0.85	0.87	6.16	6.25
150	0.93	0.89	6.78	6.66

Values of the KMPT parameters: $C_K = 0.66$, $C_M = 13.70$, and $C_P = 9.32 \times 10^{-12}$.

The temperature polarization decreases the efficiency of the process and denotes the loss of thermal energy owing to the thermal boundary layer resistance. One of the important methods to decrease the impacts of temperature polarization in the DCMD process is making the temperature at the surface of the membrane in contact with the feed side to approach the temperature of the bulk feed solution. Thus, in a high-efficiency MD system, T_m^F and T_m^P would be close to T^F and T^P, respectively, and the desired value for TPC would approach unity [21,22].

In Fig. 5, the influence of the feed temperature and velocity on the TPC is depicted. Based on Fig. 5a, the TPC shows a decreasing trend vs. temperature increase. This behavior can be owing to the exponential behavior of the vapor pressure on the feed side of the membrane which is a function of the feed temperature. The exponential growth of the vapor pressure with the feed temperature leads to a higher mass flux in the membrane, and this requires a higher amount of heat flux in the liquid phase which increases the temperature difference through the thermal boundary layers, and consequently, the TPC decreases [23]. Based on Fig. 5b, the TPC shows an increasing trend with enhancing the feed velocity (direct relationship between flow rate and TPC). This phenomenon can be studied by investigating the fluid mechanic characteristic of the fluid on the feed side. The enhancement in Re number associated with an increment in feed velocity would enhance the turbulent flow regime in the feed stream, and it causes increment in the heat transfer coefficient and decrement in the thermal boundary layer. Thus, the temperature polarization of the feed side is reduced or in other words, the TPC is increased [24].

3.4. Thermal efficiency

The heat transfer through the membrane in MD process consists of latent heat of evaporation and heat conduction across the membrane. In MD process, the contribution of the latent heat of evaporation should be increased with respect to the heat conduction. While this form of heat transfer (the latent heat of evaporation) generates water vapor, heat conduction across the membrane is deemed undesirable. In fact, the heat conduction contributes to the heat loss during MD process and should be minimized. Therefore, the thermal efficiency (TE) is a critical parameter that indicates the heat loss in the MD operation and is described as the proportion of transferred heat through the latent heat of evaporation to the total heat transfer across the membrane (latent heat plus heat conduction):

$$\mathrm{TE} = \frac{J\Delta H}{J\Delta H + \frac{k_m}{\delta_m}\left(T_m^F - T_m^P\right)} \times 100 \tag{38}$$

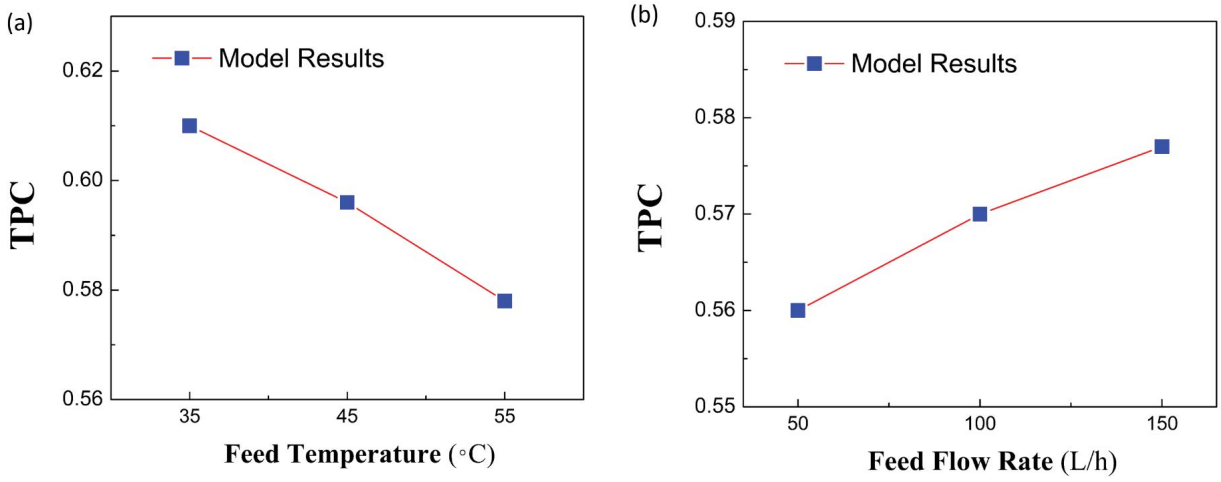

Fig. 5. Effect of (a) feed temperature and (b) velocity on the temperature polarization coefficient.

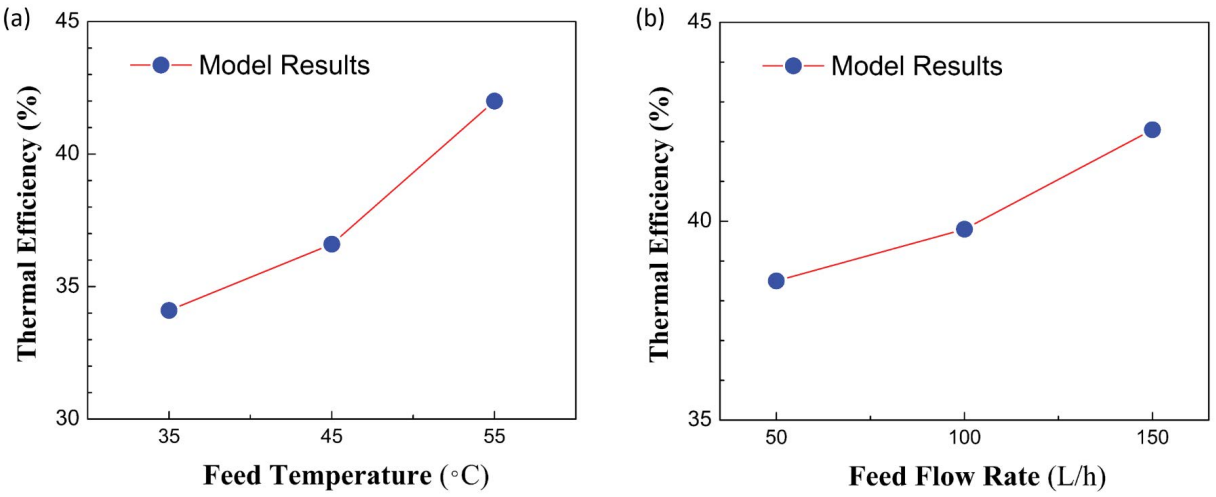

Fig. 6. Effect of (a) feed temperature and (b) velocity on the thermal efficiency.

In Fig. 6, the impact of feed temperature and velocity on the TE is depicted. Based on Fig. 6a, the TE value increases vs. increment in feed temperature. This behavior is because of the fact that the heat transfer via conduction rises linearly with temperature, whereas according to Eqs. (24) and (25), the mass transfer increases exponentially with temperature, hence the final outcome is an increment in TE with increasing the feed temperature [25,26].

Based on Fig. 6b, the TE curve indicates an increasing trend vs. enhancing the feed velocity. As mentioned, the increment in feed velocity increases the Re^F, h^F, and temperature difference across the membrane. The increment in h^F reduces the heat transfer resistance and increases the efficiency of thermal energy transfer from the feed bulk to the membrane surface. This would also lead to an increment in Re^F which would convert the flow regime from laminar to turbulent condition and improve the mixing phenomenon. Thus, the total effect of these factors would improve the water mass flux and consequently, enhances the contribution of the heat transfer for evaporation of water compared to the heat loss through conduction. This, in turn, accounts for the TE increase vs. the increment in feed flow rate [27,28].

3.5. Specific energy consumption

The specific energy consumption (SEC) is the thermal energy used for producing 1 m^3 of the product. In MD process, minimizing the amount of SEC is desirable because it implies that the process is economically feasible. This critical parameter in MD process is described as follows:

$$\mathrm{SEC} = \left[\rho_w\left(\frac{Q_t}{J}\right)\right] / 3{,}600 \tag{39}$$

$$Q_t = U\left(T^F - T^P\right) \tag{40}$$

$$U = \left[\frac{1}{h_F} + \frac{1}{\frac{k_m}{\delta_m} + \frac{J\Delta H}{\left(T_m^F - T_m^P\right)}} + \frac{1}{h_P}\right]^{-1} \tag{41}$$

In Eqs. (39) and (40), Q_t is the total heat transfer in MD operation and U is the overall heat transfer coefficient. In Fig. 7, the impact of feed temperature and velocity on SEC is indicated. Based on Fig. 7a, a decreasing trend in SEC is observed with an increment in temperature. The SEC decreased from 1,544 to 1,286 kWh/m^3 when the feed temperature rose from 35°C to 55°C at the feed flow rate of 150 L/h. The reason is that, at high feed temperatures, the thermal energy transferred through heat conduction is too small compared to the thermal energy transferred via mass flux [29,30].

According to Fig. 7b, the SEC reduces as the feed velocity increases. The SEC is decreased from 1,413 to 1,286 kWh/m^3 when the feed velocity was raised from 50 to 150 L/h. The increment in feed velocity increases the h^F, and Re^F. The increment in h^F and feed velocity results in an increase in ΔT across the membrane and the second effect of increment in feed velocity is turbulence buildup in the feed flow which enhances the mixing phenomenon and reduces the thickness of thermal boundary layer. Thus, the overall effect of these parameters is an increment in water mass flux which indicates the thermal energy transferred through the membrane via heat conduction is negligible in comparison with the heat energy transferred via water mass flux [31,32].

4. Conclusions

In this research, using experimental results and MATLAB software, two mathematical models were developed for prediction of the water mass flux in DCMD process for HFM. Prior to the calculation of the KMPT parameters (C_K, C_M, and C_P) via non-linear regression, the temperature and pressure at the liquid/membrane interface were obtained. Following the calculation of the KMPT parameters,

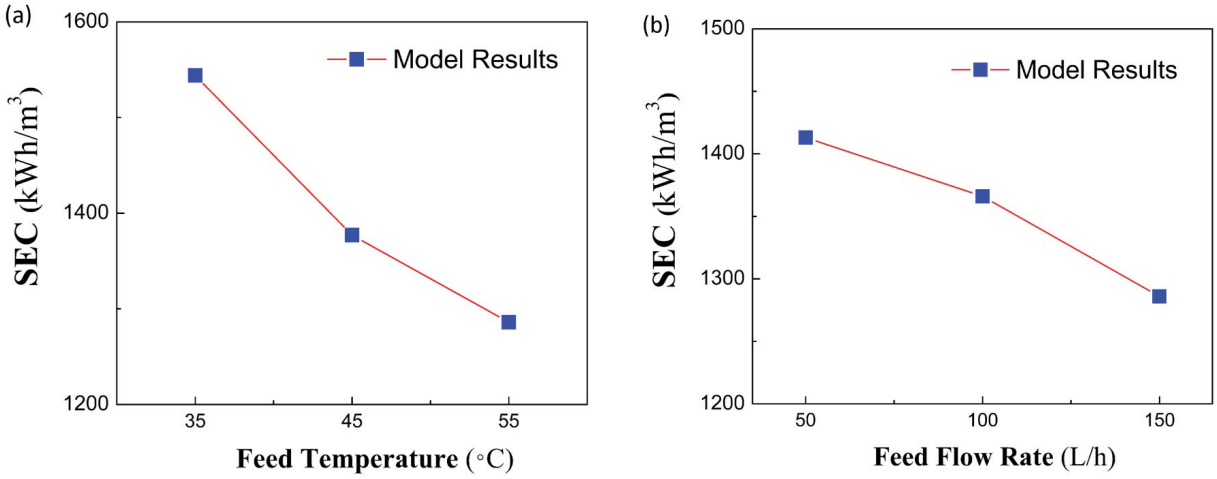

Fig. 7. Effect of (a) feed temperature and (b) velocity on the specific energy consumption.

validations of the models were confirmed through a suitable agreement between the calculated results via the KMPT model and the experimental results. Afterward, the impact of feed temperature and velocity on heat convection coefficient, TPC, TE, and SEC were probed. The models' results show that:

- Heat convection coefficient increases vs. the increment of temperature and velocity, however, the effect of velocity is more remarkable than the temperature.
- TPC parameter decreases with temperature increment. Additionally, the TPC shows an increasing trend vs. an increment in the feed velocity.
- TE parameter increases vs. temperature increment. Furthermore, TE increases vs. increment of feed velocity.
- SEC parameter decreases vs. the increment of temperature, and the SEC value decreases by enhancing feed velocity.

Symbols

C — Membrane distillation coefficient, kg/m² s Pa
C_K — Knudsen diffusion coefficient
C_M — Molecular diffusion coefficient, m
C_P — Poiseuille flow coefficient, m^{-1}
d_{lm} — Mean diameter of the fiber, m
d_i — Inner diameter of the fiber, m
d_o — Outer diameter of the fiber, m
d_h — Hydraulic diameter of the fiber, m
d_s — Inner diameter of the shell, m
I — Length of fiber, m
N — Number of fibers
D — Diffusion coefficient, m²/s
h — Heat transfer coefficient, kW/m² K
ΔH — Latent heat of vaporization, kJ/kg
J — Distillate mass flux, kg/m² s
r — Radius of membrane pore, m
K_g — Thermal conductivity of vapor–gas trapped in membrane pores, kW/m K
K_p — Thermal conductivity of the membrane material, kW/m K
K_m — Total thermal conductivity of the membrane, kW/m K
R — Gas constant, kJ/mol K
T — Temperature, K
P — Pressure, Pa
Q — Heat transfer, kW
u — Velocity, m/s
Y — Mole fraction of air in membrane pores
U — Overall heat transfer coefficient

Dimensionless numbers

Nu — Nusselt number
Pr — Prandtl number
Re — Reynolds number

Greek letters

ε — Membrane porosity
μ — Dynamic viscosity, Pa s
ρ — Density, kg/m³
Φ — Packing density
δ — Membrane thickness, m
τ — Membrane tortuosity

Superscripts

F — Feed side
P — Permeate side
m — Membrane side

Subscripts

lm — Logarithmic mean
m — Membrane side or arithmetic mean
w — Water

References

[1] M. Zamaniasl, Numerical study of direct contact membrane distillation process: effects of operating parameters on TPC and thermal efficiency, Membr. Water Treat., 10 (2019) 387–394.

[2] A. Dastbaz, J. Karimi-Sabet, H. Ahadi, Y. Amini, Preparation and characterization of novel modified PVDF-HFP/GO/ODS composite hollow fiber membrane for Caspian Sea water desalination, Desalination, 424 (2017) 62–73.
[3] K. Razmgar, E. Saljoughi, S.M. Mousavi, Preparation and characterization of a novel hydrophilic PVDF/PVA/Al_2O_3 nanocomposite membrane for removal of As(V) from aqueous solutions, Polym. Compos., 40 (2019) 2452–2461.
[4] A. Alkhudhiri, N. Darwish, N. Hilal, Membrane distillation: a comprehensive review, Desalination, 287 (2012) 2–18.
[5] E. Karbasi, J. Karimi-Sabet, J. Mohammadi-Rovshandeh, M.A. Moosavian, H. Ahadi, Y. Amini, Experimental and numerical study of air-gap membrane distillation (AGMD): novel AGMD module for Oxygen-18 stable isotope enrichment, Chem. Eng. J., 322 (2017) 667–678.
[6] J. Zahirifar, A. Hadi, J. Karimi-Sabet, A. Dastbaz, Influence of hexagonal boron nitride nanosheets as the additives on the characteristics and performance of PVDF for air gap membrane distillation, Desalination, 460 (2019) 81–91.
[7] J. Zahirifar, J. Karimi-Sabet, S.M.A. Moosavian, A. Hadi, P. Khadiv-Parsi, Fabrication of a novel octadecylamine functionalized graphene oxide/PVDF dual-layer flat sheet membrane for desalination via air gap membrane distillation, Desalination, 428 (2018) 227–239.
[8] K.W. Lawson, D.R. Lloyd, Membrane distillation, J. Membr. Sci., 124 (1997) 1–25.
[9] E. Drioli, A. Ali, F. Macedonio, Membrane distillation: recent developments and perspectives, Desalination, 356 (2015) 56–84.
[10] L.M. Camacho, L. Dumée, J. Zhang, J.-d. Li, M. Duke, J. Gomez, S. Gray, Advances in membrane distillation for water desalination and purification applications, Water, 5 (2013) 94–196.
[11] T. Vazirnejad, J. Karimi-Sabet, A. Dastbaz, M.A. Moosavian, S.A. Ghorbanian, Application of salt additives and response surface methodology for optimization of PVDF hollow fiber membrane in DCMD and AGMD processes, J. Membr. Sci. Res., 2 (2016) 169–178.
[12] P. Yazgan-Birgi, M.I.H. Ali, H.A. Arafat, Comparative performance assessment of flat sheet and hollow fiber DCMD processes using CFD modeling, Sep. Purif. Technol., 212 (2019) 709–722.
[13] H. Yu, X. Yang, R. Wang, A.G. Fane, Numerical simulation of heat and mass transfer in direct membrane distillation in a hollow fiber module with laminar flow, J. Membr. Sci., 384 (2011) 107–116.
[14] H. Yu, X. Yang, R. Wang, A.G. Fane, Analysis of heat and mass transfer by CFD for performance enhancement in direct contact membrane distillation, J. Membr. Sci., 405 (2012) 38–47.
[15] L.-H. Cheng, P.-C. Wu, J. Chen, Modeling and optimization of hollow fiber DCMD module for desalination, J. Membr. Sci., 318 (2008) 154–166.
[16] Z. Ding, R. Ma, A. Fane, A new model for mass transfer in direct contact membrane distillation, Desalination, 151 (2003) 217–227.
[17] Y.-D. Kim, Y.-B. Kim, S.-Y. Woo, Detailed modeling and simulation of an out-in configuration vacuum membrane distillation process, Water Res., 132 (2018) 23–33.
[18] V. Perfilov, A. Ali, V. Fila, A general predictive model for direct contact membrane distillation, Desalination, 445 (2018) 181–196.
[19] M.M. Teoh, S. Bonyadi, T.-S. Chung, Investigation of different hollow fiber module designs for flux enhancement in the membrane distillation process, J. Membr. Sci., 311 (2008) 371–379.
[20] J. Zhang, S. Gray, Modelling heat and mass transfers in DCMD using compressible membranes, J. Membr. Sci., 387 (2012) 7–16.
[21] A. Ali, F. Macedonio, E. Drioli, S. Aljlil, O. Alharbi, Experimental and theoretical evaluation of temperature polarization phenomenon in direct contact membrane distillation, Chem. Eng. Res. Des., 91 (2013) 1966–1977.
[22] X. Yang, H. Yu, R. Wang, A.G. Fane, Analysis of the effect of turbulence promoters in hollow fiber membrane distillation modules by computational fluid dynamic (CFD) simulations, J. Membr. Sci., 415 (2012) 758–769.
[23] A. Kurdian, M. Bahreini, G. Montazeri, S. Sadeghi, Modeling of direct contact membrane distillation process: flux prediction of sodium sulfate and sodium chloride solutions, Desalination, 323 (2013) 75–82.
[24] P. Moghaddam Kamrani, O. Bakhtiari, P. Kazemi, T. Mohammadi, Theoretical modeling of direct contact membrane distillation (DCMD): effects of operation parameters on flux, Desal. Water Treat., 56 (2015) 2013–2022.
[25] Y. Zhang, Y. Peng, S. Ji, Z. Li, P. Chen, Review of thermal efficiency and heat recycling in membrane distillation processes, Desalination, 367 (2015) 223–239.
[26] J. Zhang, M. Duke, M. Hoang, Z. Xie, A. Groth, C. Tun, S. Gray, Influence of module design and membrane compressibility on VMD performance, J. Membr. Sci., 442 (2013) 31–38.
[27] Z. Li, Y. Peng, Y. Dong, H. Fan, P. Chen, L. Qiu, Q. Jiang, Effects of thermal efficiency in DCMD and the preparation of membranes with low thermal conductivity, Appl. Surf. Sci., 317 (2014) 338–349.
[28] S. Al-Obaidani, E. Curcio, F. Macedonio, G. Di Profio, H. Al-Hinai, E. Drioli, Potential of membrane distillation in seawater desalination: thermal efficiency, sensitivity study and cost estimation, J. Membr. Sci., 323 (2008) 85–98.
[29] M. Khayet, Solar desalination by membrane distillation: dispersion in energy consumption analysis and water production costs (a review), Desalination, 308 (2013) 89–101.
[30] K. Okiel, A.H.M. El-Aassar, T. Temraz, S. El-Etriby, H.A. Shawky, Vacuum enhanced direct contact membrane distillation for oil field produced water desalination: specific energy consumption and energy efficiency, Desal. Water Treat., 57 (2016) 11945–11955.
[31] M.R. Elmarghany, A.H. El-Shazly, M.S. Salem, M.N. Sabry, N. Nady, Thermal analysis evaluation of direct contact membrane distillation system, Case Stud. Therm. Eng., 13 (2019), 100377 doi: 10.1016/j.csite.2018.100377.
[32] G. Zaragoza, A. Ruiz-Aguirre, E. Guillén-Burrieza, Efficiency in the use of solar thermal energy of small membrane desalination systems for decentralized water production, Appl. Energy, 130 (2014) 491–499.